ACS OMEGA

Open Access

http://pubs.acs.org/journal/acsodf

Article

Experimental and Molecular Dynamics Simulation Insights into Adsorption of Co(II), Cr(III), and Cu(II) on Chitosan and Chitosan/Tripolyphosphate Nanoparticles

Malinee Promkatkaew, Supaporn Baiya, Suree Tongwanichniyom, and Sunan Kitjaruwankul*

Cite This: *ACS Omega* 2024, 9, 4019−4026

Read Online

ACCESS | Metrics & More | Article Recommendations

ABSTRACT: Chitosan (CS)/tripolyphosphate (TPP) nanoparticles were synthesized using the ionic gelation method based on the mass ratio and volume ratio between CS and TPP and then subsequently characterized using XRD, FT-IR, and SEM. The interaction between the metal ions Co(II), Cr(III), and Cu(II) on CS and 2CS/TPP was simulated using molecular dynamics (MD), and the findings were compared with the experimental data. CS/TPP nanoparticles were more favorable than using pure chitosan at a % removal efficiency of 91.47, 89.11, and 78.11 for Cu(II), Cr(III), and Co(II), respectively. The binding energy between 2CS/TPP and the metals was more favorable than that for CS at −214.95, −106.87, and −58.11 kcal/mol for Cr(III), Co(II), and Cu(II), respectively. The CS/TPP nanoparticles greatly affect metal adsorption and are therefore considered materials for wastewater treatment.

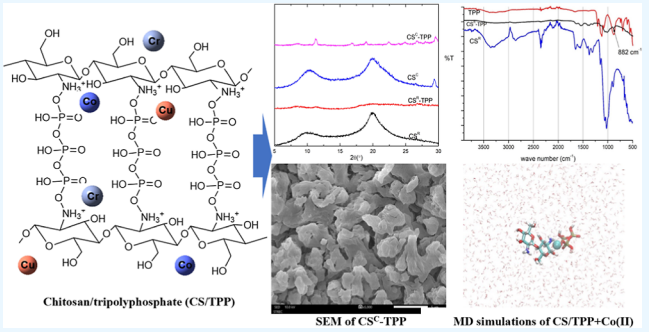

1. INTRODUCTION

Over the last 30 years, electronic devices, such as mobile phones, smart TVs, desktop PCs, microwave ovens, and air conditioners, have been developed continuously according to the needs of people. This has resulted in many metals being used in electrical manufacturing that can be released into the environment. Specifically, the toxic metals from waste electrical and electronic equipment (WEEE) are widely known as e-waste.[1] WEEE samples (collected in 2009) covered 54 metals, consisting of Ag, Al, As, Au, B, Ba, Be, Bi, Ca, Cd, Ce, Co, Cr, Cs, Cu, Dy, Eu, Fe, Ga, Ge, Hf, In, Ir, K, La, Li, Mg, Mn, Mo, Na, Nb, Nd, Ni, Pb, Pd, Pt, Rb, Rh, Ru, Sb, Sc, Se, Si, Sn, Sr, Ta, Te, Ti, Tl, V, W, Y, Zn, and Zr, determined using inductively coupled plasma-optical emission spectroscopy (ICP-OES) and inductively coupled plasma−mass spectrometry (ICP−MS).[2] These toxic metals cause a potential environmental impact; consequently, many research groups have been interested in developing removal methods for keeping the number of discharged metals as low as possible. There are many conventional methods for removing toxic metals, such as adsorption, precipitation, and ion exchange.[3−7] Among these methods, adsorption based on a low-cost and environmentally friendly absorbent has been of particular interest.

Chitosan (CS) is a natural adsorbent used in various pollutants for metal removal. CS can be extracted from shrimp shells or crab shells using demineralization, deproteination, and diacylation.[8] The structure of chitosan is divided into two parts of glucose amine and *N*-acetyl glucosamine composed of (1,4)-linked 2-amino-2-deoxy-*β*-D-glucan, whose chemical name is poly[-(1,4)-2-amino-2-deoxy-D-glucopyranose].[9] Both amine and hydroxyl groups in CS can chelate with metal due to their electron-donating groups; therefore, CS has been widely used as a candidate for wastewater treatment.[10−12]

CS nanoparticles can be synthesized using several methods, such as electrospraying, emulsification, solvent diffusion, microemulsion, and ionic gelation.[13] Ionic gelation or ion-induced gelation consists of the spontaneous reaction of cationic chitosan with an anionic cross-linking agent, usually tripolyphosphate (TPP), forming a polyelectrolyte complex named CS/TPP. This complex is stabilized by cross-linked electrostatic interaction between the CS−NH_3^+ and TPP−O groups, resulting in a three-dimensional entanglement that precipitates from an aqueous solution in the form of gel-like nanoparticles.[14,15] Considering that glucosamine groups are pH-sensitive ($pK_a \approx 6$), TPP/CS nanoparticles are synthesized in a dilute aqueous acidic solution (pH < 6.5) that can be

Received: November 7, 2023
Revised: December 21, 2023
Accepted: December 26, 2023
Published: January 8, 2024

converted to glucosamine units in the soluble form of protonated amine ($R-NH_2 + H^+ \rightarrow R-NH_3^+$).[16] Recently, other attractive materials of metal−organic frameworks (MOFs) have been used for removing pesticides (2,4-dichlorophenyl acetic acid),[17] tetracycline,[18] doxorubicin hydrochloride,[19] tartrazine food dye,[20] and two sulfa drugs, i.e., sulfamethazine and sulfanilamide[21] from wastewater, which provided the high efficiency and reusable adsorbents. Moreover, the interesting natural adsorbent of cellulose nanofiber composites can be used to recover Co(II) from battery waste and remove it from wastewater with an effective limit of detection (LOD) of 0.87 ppb.[22]

Molecular dynamics (MD) simulations have become valuable tools for understanding the nature of interactions and binding affinity in supramolecular systems. Density functional levels of theory such as DFT[11,23] have been used to study metal adsorption complexes. Our previous research[24] performed DFT-based analysis to study the metal adsorption with Ag^+, As^{3+}, Ba^{2+}, Be^{2+}, Cd^{2+}, Co^{2+}, Cr^{3+}, Cu^{2+}, Hg^{2+}, Li^+, Mn^{2+}, Ni^{2+}, Pb^{2+}, Pd^{2+}, Sb^{3+}, Sn^{2+}, Sr^{2+}, Tl^+, and Zn^{2+} on a CS monomer, indicating all the studied metals were placed closer to an N atom than an O atom in CS due to the higher Schiff-based property of an N atom compared to that of an O atom.

The current work synthesized CS/TPP nanoparticles based on the ionic gelation method with the mass ratio and volume ratio between CS and TPP as displayed in Figure 1, as

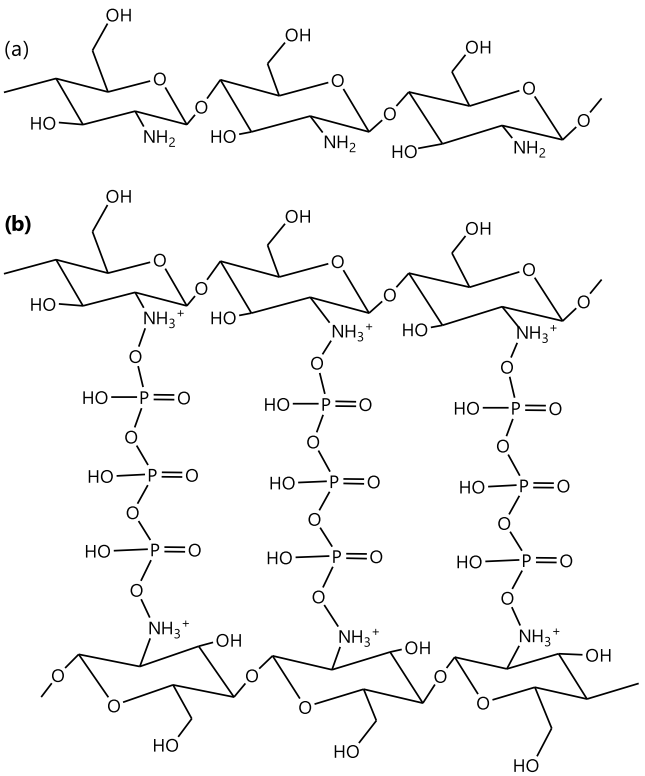

Figure 1. Structures of (a) chitosan (CS) and (b) chitosan/tripolyphosphate (CS/TPP) composites.

previously reported.[13] MD simulations are an attractive method to gain a good understanding of the atomic-level structure, involving Newton's law of motion and appropriate algorithms to solve the momentum and velocity of every atom simulated in the studied system. The current study aimed to investigate the interactions between some metal ions, Co(II), Cr(III), and Cu(II), on the CS monomer (1CS), CS oligomer (9CS), and dimer CS/TPP (2CS/TPP) through MD simulations compared with those of the wet experiment using the adsorption power of CS and CS/TPP nanoparticles.

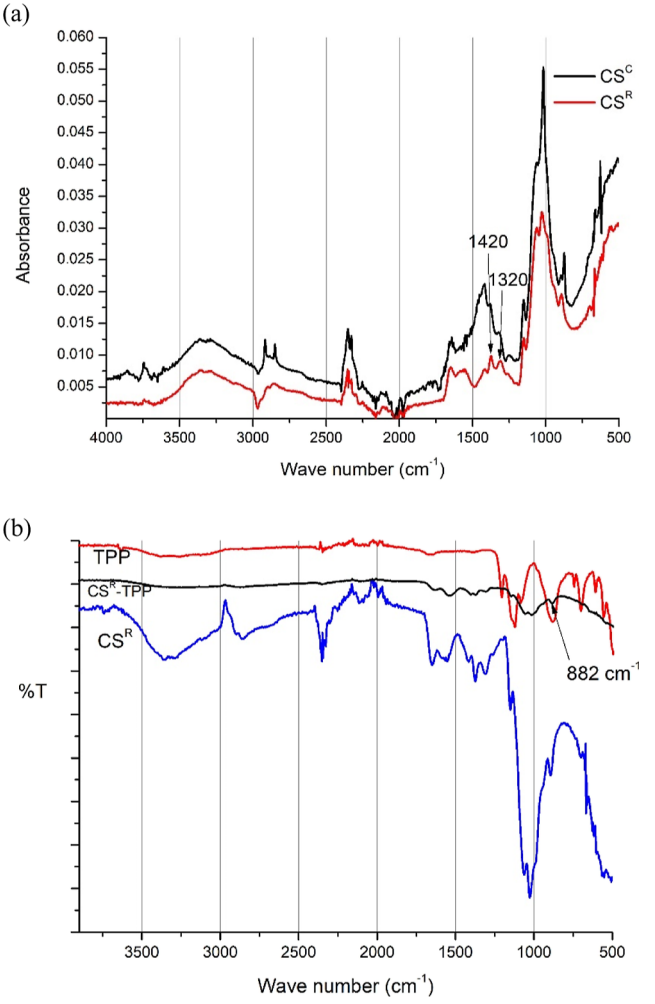

Figure 2. (a) FT-IR absorption spectra of CS^C and CS^R and (b) FT-IR transmittance spectra of CS^R, TPP, and CS^R/TPP.

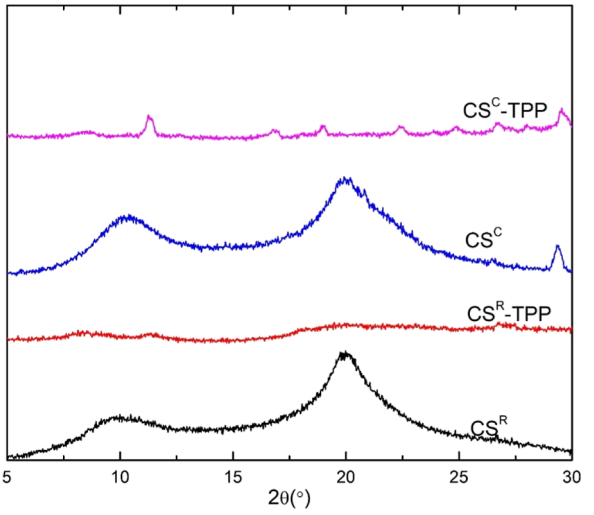

Figure 3. XRD pattern of CS^C, CS^R, CS^C/TPP, and CS^R/TPP composites.

https://doi.org/10.1021/acsomega.3c08835
ACS Omega 2024, 9, 4019−4026

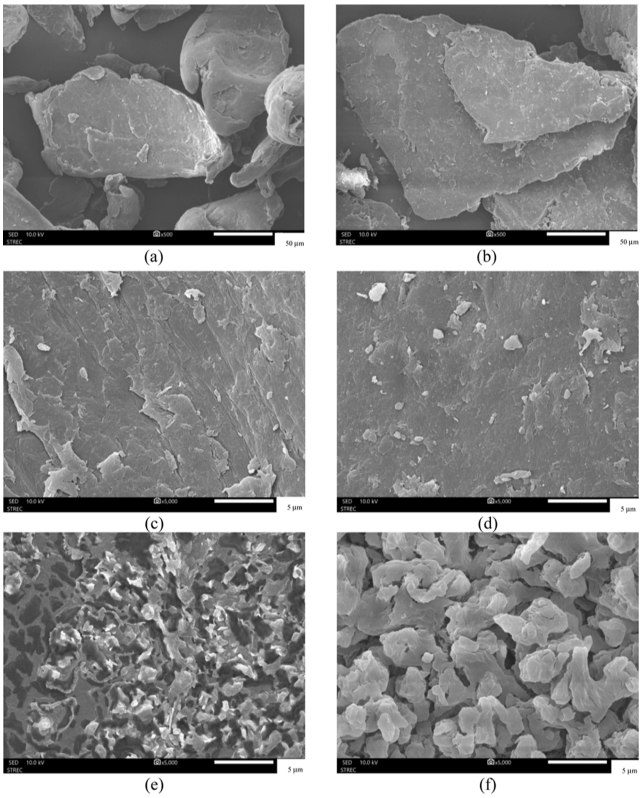

Figure 4. SEM images of pure chitosan (a) CS^R and (b) CS^C at 500× magnification, (c) CS^R and (d) CS^C at 5000× magnification, and CS/TPP composites (e) CS^R/TPP and (f) CS^C/TPP at 5000× magnification.

Table 1. % Removal Efficiency (% RE) at 120 min and the Optimum pH of Each Metal Adsorption

		% RE ± SD (n = 3)		
metal	optimum pH	CS^R	CS^R/TPP	CS^C/TPP
Co(II)	9	50.33 ± 0.02	59.22 ± 0.06	78.11 ± 0.01
Cr(III)	8	75.41 ± 0.05	85.41 ± 0.05	89.11 ± 0.06
Cu(II)	7	74.29 ± 0.04	88.13 ± 0.02	91.47 ± 0.01

2. EXPERIMENTAL SECTION

2.1. Materials. Two types of CS were used, i.e., CS reagent grade (Sigma-Aldrich; low molecular weight with a percentage of the degree of deacetylation (% DD) of 76% and abbreviated as CS^R) and CS commercial grade (purchased from an agricultural store and abbreviated as CS^C). 1,10-Phenantroline monohydrate (Loba Chemie) and $Na_5P_3O_{10}$ (sodium tripolyphosphate; TPP) were purchased from Alfa Aesar. $CrCl_3{\cdot}6H_2O$ and $CoCl_2{\cdot}6H_2O$ were purchased from Laba. $Cu(NO_3)_2{\cdot}6H_2O$ was purchased from Carlo. Other reagents, such as CH_3COOH, CH_3COONa, NaOH, and HCl, were all of analytical grade.

2.2. Synthesis of CS/TPP-NPs. Samples of 1% (w/v) of chitosan were prepared by adding 3 g of CS powder into 300 mL of 1%(w/v) of acetic acid under stirring (adjusted pH to 5 using 1 M NaOH) until obtaining a clear solution (ca. 40 min) and then slowly adding 100 mL of 0.1% (w/v) of TPP (adjusted pH to 5 using 0.1 M HCl) into the chitosan solution under stirring until a gel formed (ca. 2 h).

2.3. Characterization. The functional group of the structure was identified based on attenuated total reflectance Fourier transform infrared spectroscopy (ATR-FT-IR; Bruker Invenio R). The crystal pattern was determined based on the X-ray diffractometry (XRD; Bruker D8 DISCOVER, Cu Kα) using a voltage of 40 kV and a current of 40 mA with a scanning of 1−80°. Morphology was elucidated using scanning electron microscopy (SEM; JEOL JSM-IT300) at an applied voltage of 10 kV.

2.4. Batch Adsorption Experiments. Co(II), Cr(III), and Cu(II) were used to study the adsorption performance of CS^R, CS^R/TPP, and CS^C/TPP. First, we evaluated the effects of contact times of 30, 60, and 120 min with Co(II) adsorption using 0.1 g of CS^R into a 10 mL aliquot of standard 100 ppm of Co(II). Then, we investigated the optimal pH values at 7, 8, and 9. After the mixture was stirred for each studied contact time, the supernatant was filtered. The concentration of the remaining metal was determined by complexing with 1,10-phenanthroline, which is a common ligand used for complexing many metal ions[25−27] and then measuring the absorbance of the metal-complex at a maximum wavelength for Co(II)-complex at 511 nm, Cr(III)-complex at 426 nm, and Cu(II)-complex at 812 nm. The remaining concentration of each metal was calculated by using the calibration curve with a linear range of 5−50 ppm. After that, we performed separate batch adsorptions for Co(II), Cr(III), and Cu(II) with the other adsorbents of CS^R/TPP and CS^C/TPP at the optimum pH and contact time. The % removal efficiency (% RE) was

Table 2. RMSD Values of the Studied Systems

	RMSD (Å)			
metal	1CS	9CS	2CS	TPP
Co(II)	0.6	3.0	1.0	0.8
Cr(III)	0.6	4.0	1.0	0.8
Cu(II)	0.6	4.0	1.0	0.8

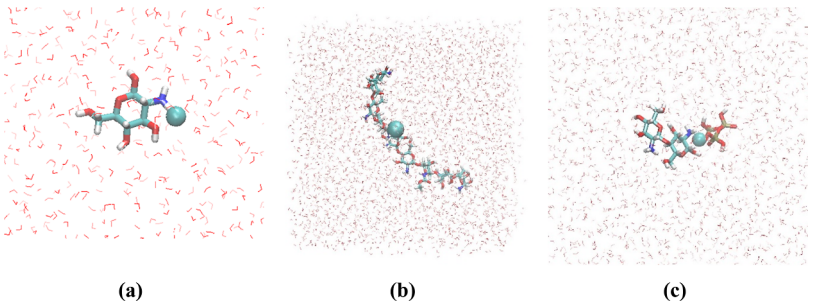

Figure 5. Structural system of (a) 1CS + Co(II), (b) 9CS + Co(II), and (c) 2CS/TPP + Co(II).

https://doi.org/10.1021/acsomega.3c08835
ACS Omega 2024, 9, 4019−4026

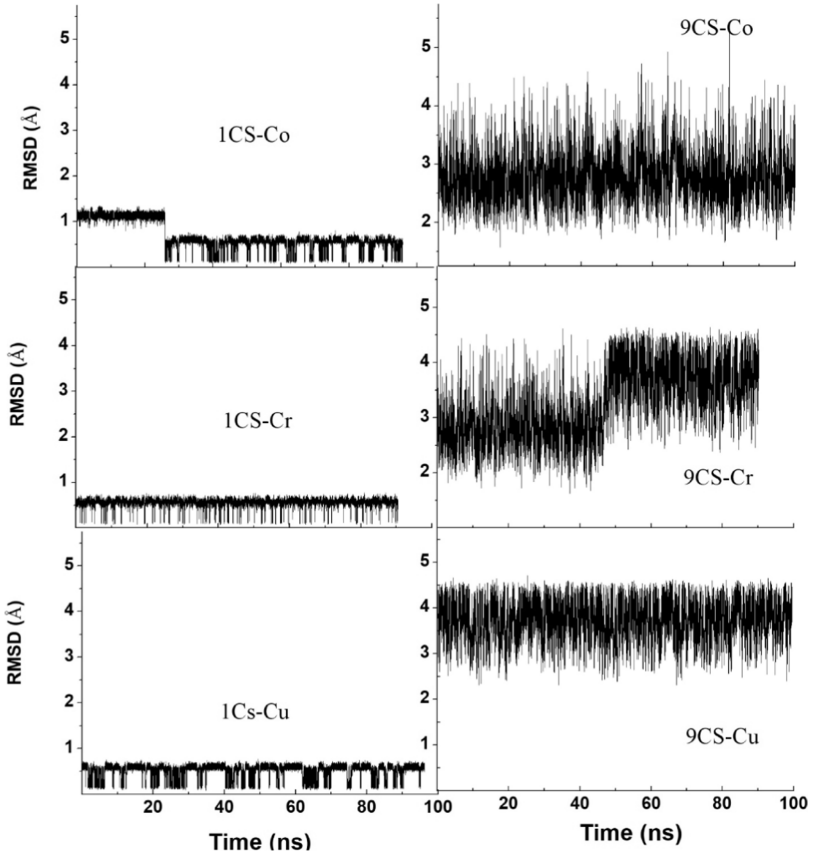

Figure 6. RMSD values of (a) 1CS + Co(II), (b) 1CS + Cr(III), (c) 1CS + Cu(II), (d) 9CS + Co(II), (e) 9CS + Cr(III), and (f) 9CS + Cu(II).

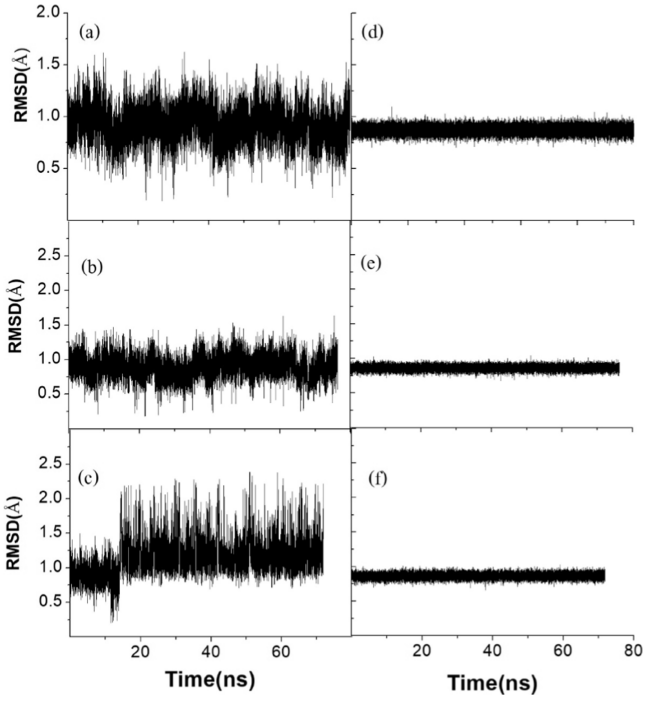

Figure 7. RMSD values of 2CS/TPP systems. (a–c) 2CS of Co(II), Cr(III), and Cu(II), respectively. (d–f) TPP of Co(II), Cr(III), and Cu(II), respectively.

calculated using eq 1, where C_0 is the initial concentration and C_e is the concentration after adsorption

$$\% \text{ RE} = \left(\frac{C_0 - C_e}{C_0}\right) \times 100 \quad (1)$$

2.5. MD Simulation Details. MD simulations of metals–CS were carried out using the NAMD v.2.14 software.[28] A Swiss Param server[29] was used to calculate the force-field parameters and topology of CS. The PSF file was generated using the VMD molecular graphics program v.1.9.4.[30] CS of each system included a monomer of CS (1CS), an oligomer of 9 CS units (9CS), and a dimer of the CS/TPP composite (2CS/TPP). The metal–chitosan complex was solved with cubic water boxes containing transferable intermolecular potential with 3 points (TIP3P) water molecules.[31] The size of a simulation box was determined to be 15 Å between the metal–chitosan surface and the edges of the periodic box. A cutoff radius for nonbonded interactions was calculated as 12 Å. The particle mesh Ewald (PME)[32] method was used to calculate long-range electrostatic interactions. The SHAKE algorithm[33] was used to constrain all bonds involving hydrogen atoms. First, the system was minimized for 50,000 steps of steepest descent and then heated from 50 to 300 K while restraining the CS backbone and metal atom. After that, the CS backbone and metal atom were gradually released and equilibrated at 300 K for 5 ns. The production MD run was performed by using an *NPT* ensemble. The Nosé–Hoover method[34] was used to maintain a constant temperature. The simulation time step was set to 2 fs. The simulation time was 200 ns. The binding energy between CS and metal was calculated using the molecular mechanics Poisson–Boltzmann surface area (MM/PBSA) method with the CaFE (calculation of free energy) plugin.[35]

https://doi.org/10.1021/acsomega.3c08835
ACS Omega 2024, 9, 4019–4026

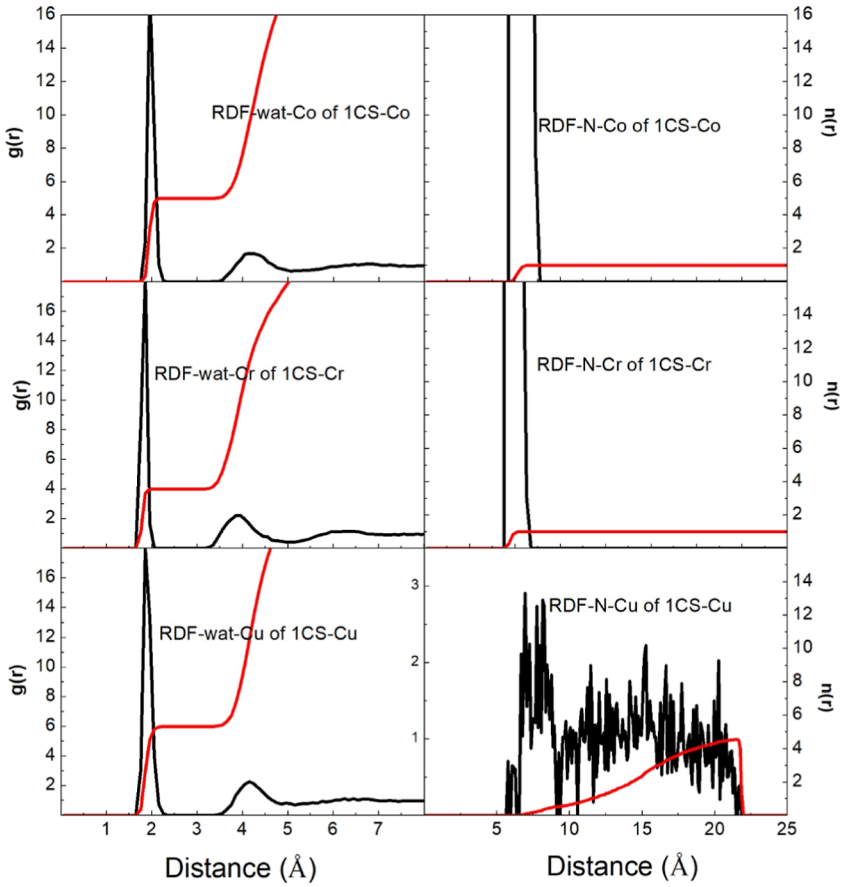

Figure 8. RDFs of the 1CS−metal systems.

Table 3. Binding Energy ($\Delta G_{binding}$) between the Metal and Adsorbent

	$\Delta G_{binding}$ (kcal/mol)		
metal	1CS	9CS	2CS/TPP
Co(II)	−9.54	−15.25	−106.87
Cr(III)	−43.62	−5.85	−214.95
Cu(II)	−1.56	−1.80	−58.11

Table 4. RDF of the 1CS and 9CS Metal Systems[a]

	1CS			9CS		
metal	CN of water	CN of N (CS)	CN of O (CS)	CN of water	CN of O (CS)	CN of N (CS)
Co(II)	5	1	0	4	1	1
Cr(III)	4	1	1	4	1	1
Cu(II)	6	0	0	4	1	1

[a]Note: CN refers to the coordination number.

3. RESULTS AND DISCUSSION

3.1. FT-IR Results. The % DD was calculated using the absorption bands at 1320 and 1420 cm^{-1} from FT-IR, where the first was characteristic of the acetylated amine or amide function, and the second band was chosen as the reference band.[36]

$$\%\ DD = 100 - \left(\frac{A_{1320}}{A_{1420}} - 0.3822\right) \times \frac{1}{0.03133} \quad (2)$$

The FT-IR absorption spectra of CS^C and CS^R and the FT-IR transmittance spectra of CS^R, TPP, and CS^R/TPP are shown in Figure 2. The obtained % DD of CS^R was 75.31%, corresponding to the information on Sigma-Aldrich certification (76%), and for CS^C, the % DD was 91.56%. Thus, it could be considered that CS^C was a high MW CS. CS/TPP had a decreased band at 3360 cm^{-1}, which was attributed to the −NH overlapping with −OH stretching and indicating the occurrence of cross-linking. In addition, the peak at 882 cm^{-1} confirmed the functional group of phosphate oxygen bonding (P−O−P), corresponding to an antisymmetric stretching of the P−O−P bridge.[37]

3.2. XRD Pattern. The obtained XRD patterns are displayed in Figure 3. The 2ι-peaks at 10 and 20° of both chitosan standards indicated the crystal planes of (020) and (110), respectively. These results were in good agreement with other works showing the characteristic peaks referring to JCPDS no. 39-1894,[38,39] while the intensity of these two peaks decreased in the XRD pattern of the CS/TPP composites due to the occurrence of the amorphous structure, in agreement with the previous study.[12]

3.3. SEM Results. SEM images of pure CS (CS^R and CS^C) at 500× magnification and 5000× magnification are shown in Figure 4, displaying a nonporous and flat sheet structure consistent with a previous study.[40] The different structures observed for CS/TPP are also shown in Figure 4 at 500× magnification. CS^C/TPP had a higher porosity than that of CS^R/TPP, and at 5000× magnification, it was apparent that CS^C/TPP had a more homogeneous size compared to that of CS^R/TPP, while both CS/TPP types had a more amorphous

https://doi.org/10.1021/acsomega.3c08835
ACS Omega 2024, 9, 4019−4026

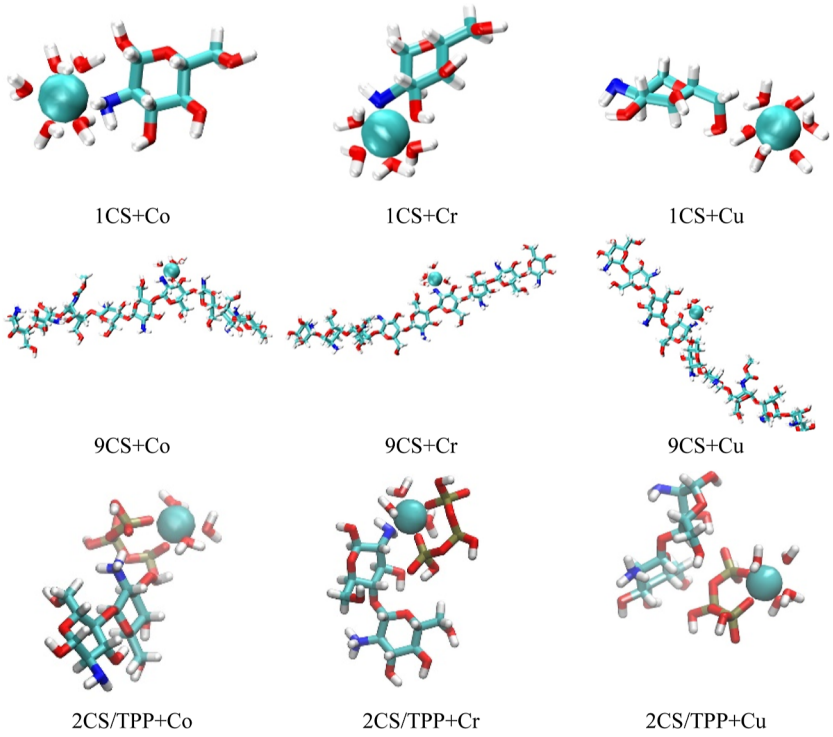

Figure 9. Diagrammatic representations of all of the studied systems. Cyan is the C atom, blue is the N atom, red is the O atom, and white is the H atom.

structure than that of the neat CS, which corresponded with the XRD results. Our CS/TPP morphology was consistent with other works.[41,42]

3.4. Removal Efficiency. After determining the optimum contact time from the adsorption of metal ions (120 min), we performed batch adsorption of each metal using CS^R 0.1 g to evaluate the optimum pH (7, 8, or 9). The % RE results at 120 min and the optimum pH of each of the Co(II), Cr(III), and Cu(II) metal adsorptions are shown in Table 1. The CS^C/TPP composites provided the highest removal efficiency because composites with TPP increased the anion of the phosphate groups on the adsorbent, which was also consistent with CS^C having a higher % DD (91.56%) than CS^R (75.31%). Notably, we did not perform the metal adsorption with an acidic medium because CS can be protonated at the $-NH_2$ group, resulting in competition between the metal ions and protons for adsorption sites, as reported elsewhere.[43]

3.5. MD Results and Structural Stability over Simulation Time. We performed MD simulations of metal−CS in water solvation to gain insight into the atomistic interaction between the metal ions and CS. The modeled adsorbents were a monomer of CS (1CS), an oligomer of 9 CS units (9CS), and a dimer of the CS/TPP composite (2CS/TPP), as shown in Figure 5. The root-mean-square-deviation (RMSD) values of the CS backbones were calculated and compared to those of the initial structure over the simulation time. The obtained RMSD value was 1.2 Å at the beginning of the production run for the mono 1CS−Co system and stabilized at about 2.2 Å over 100 ns of simulation time. The other systems provided stable RMSD values, as reported in Table 2 and Figures 6 and 7 over the simulation times, indicating that the studied system had equilibrated. In addition, we calculated the RDF values to investigate the coordination numbers of O(water)−metal, O(CS)−metal, and N(CS)−metal. This work showed that the first shell distances of Cu(II) and Cr(III) were 1.85 Å, and for Co(II), the distance was 1.95 Å, as shown in Figure 8. All the metal ions have octahedral configurations that agree well with the previous study.[44] Although Cu(II) was not coordinated with CS, it had the lowest binding energy ($\Delta G_{binding}$), as shown in Table 3. Furthermore, the RDF values of the 9CS−metal systems revealed that the second shell structure of all CS−metal complexes had an octahedral structure, with the coordination numbers shown in Table 4. Cr(III) coordinated with both the N atom and the O atom of CS, while Co(II) coordinated with the N atom of CS. However, Cu(II) did not coordinate with CS directly, as shown in Figure 9.

The binding energy from the trajectory between metal and adsorbent was calculated based on the MM/PBSA method,[45] where the difference in energy in the gas phase between the complex and the separated receptor and the ligand was calculated using NAMD. Then, the polar solvation-free energy was calculated using the Poisson−Boltzmann (PB) equation using APBS.[46] After that, the difference between the solvent-accessible surface area (SASA) and the nonpolar solvation-free energy was estimated based on the linear relation approximated using SASA. Finally, the net binding free energy (ΔG) was calculated in which the entropic term has a high computational cost that can be ignored in the calculation according to eq 3

$$\Delta G = \Delta H - T\Delta S = \langle \Delta E_{gas} + \Delta G_{sol}{}^{polar} + \Delta G_{sol}{}^{non-polar} - T\Delta S \rangle \quad (3)$$

where the G term can be further decomposed into eq 4

$$\Delta G_{binding} = G_{cpx} - (G_{receptor} + G_{ligand}) \quad (4)$$

https://doi.org/10.1021/acsomega.3c08835
ACS Omega 2024, 9, 4019−4026

where cpx refers to the complex, the receptor refers to an adsorbent, and the ligand refers to a metal ion.

The negative binding energy results indicated that all the studied metals attractively interacted with CS and the CS/TPP composite. The Cr(III) complex with 2CS/TPP had the lowest binding energy supported by the strong composite between 2CS and TPP. Compared to the experimental results of % RE using the CS/TPP composite, the highest removal efficiency was for the adsorption of Cu(II) (91.47%). However, the RDF and binding energy revealed the opposite result for Cu(II) adsorption not being CS-coordinated but having a lower negative binding energy. Although the theoretical results did not completely correlate with our experimental results, the MD simulation results confirmed that there was coordination between CS and the studied metal ions. The binding energy between the 2CS/TPP composite of each metal ion was more favorable than that of the pure CS adsorption, which was consistent with the experimental results.

4. CONCLUSIONS

CS/TPP nanoparticles were successfully synthesized and characterized and then used as an adsorbent for removing three metal ions: Co(II), Cr(III), and Cu(II). CS/TPP nanoparticles were more favorable than using pure chitosan at percentage removal efficiencies of 91.47, 89.11, and 78.11 for Cu(II), Cr(III), and Co(II), respectively. According to MD simulations, the binding energies between 2CS/TPP and the metals were found to be Cr(III) > Co(II) > Cu(II). They suggested that there were molecular interactions among CS, TPP, and the three studied metal ions, which should provide insight into the adsorption mechanism.

AUTHOR INFORMATION

Corresponding Author

Sunan Kitjaruwankul − *Faculty of Science at Sriracha, Kasetsart University Sriracha Campus, Chonburi 20230, Thailand;* orcid.org/0000-0002-5506-9510; Email: srcsnk@ku.ac.th

Authors

Malinee Promkatkaew − *Faculty of Science at Sriracha, Kasetsart University Sriracha Campus, Chonburi 20230, Thailand*

Supaporn Baiya − *Faculty of Science at Sriracha, Kasetsart University Sriracha Campus, Chonburi 20230, Thailand*

Suree Tongwanichniyom − *Faculty of Science at Sriracha, Kasetsart University Sriracha Campus, Chonburi 20230, Thailand*

Complete contact information is available at: https://pubs.acs.org/10.1021/acsomega.3c08835

Notes

The authors declare no competing financial interest.

ACKNOWLEDGMENTS

This work was supported by the Faculty of Science at Sriracha (Sci-SrcG03/2565), Kasetsart University Sriracha campus, and the Kasetsart University Research and Development Institute (KURDI), Thailand, through the provision of partial support and research facilities.

REFERENCES

(1) Marinello, S.; Gamberini, R. Multi-Criteria Decision Making Approaches Applied to Waste Electrical and Electronic Equipment (WEEE): A Comprehensive Literature Review. *Toxics* **2021**, *9*, 13.

(2) Oguchi, M.; Sakanakura, H.; Terazono, A. Toxic Metals in WEEE: Characterization and Substance Flow Analysis in Waste Treatment Processes. *Sci. Total Environ.* **2013**, *463*−*464*, 1124−1132.

(3) Qasem, N. A. A.; Mohammed, R. H.; Lawal, D. U. Removal of Heavy Metal Ions from Wastewater: A Comprehensive and Critical Review. *npj Clean Water* **2021**, *4*, 36.

(4) Kakaei, S.; Khameneh, E. S.; Rezazadeh, F.; Hosseini, M. H. Heavy Metal Removing by Modified Bentonite and Study of Catalytic Activity. *J. Mol. Struct.* **2020**, *1199*, 126989.

(5) Masood, N.; Irshad, M. A.; Nawaz, R.; Abbas, T.; Abdel-Maksoud, M. A.; AlQahtani, W. H.; AbdElgawad, H.; Rizwan, M.; Abeed, A. H. A. Green Synthesis, Characterization and Adsorption of Chromium and Cadmium from Wastewater Using Cerium Oxide Nanoparticles; Reaction Kinetics Study. *J. Mol. Struct.* **2023**, *1294*, 136563.

(6) Pohl, A. Removal of Heavy Metal Ions from Water and Wastewaters by Sulfur-Containing Precipitation Agents. *Water Air Soil Pollut.* **2020**, *231*, 503.

(7) Bashir, A.; Malik, L. A.; Ahad, S.; Manzoor, T.; Bhat, M. A.; Dar, G. N.; Pandith, A. H. Removal of Heavy Metal Ions from Aqueous System by Ion-Exchange and Biosorption Methods. *Environ. Chem. Lett.* **2019**, *17*, 729−754.

(8) Varun, T. K.; Senani, S.; Jayapal, N.; Chikkerur, J.; Roy, S.; Tekulapally, V. B.; Gautam, M.; Kumar, N. Extraction of Chitosan and Its Oligomers from Shrimp Shell Waste, Their Characterization and Antimicrobial Effect. *Vet. World* **2017**, *10*, 170−175.

(9) Zia, Q.; Tabassum, M.; Gong, H.; Li, J. A Review on Chitosan for the Removal of Heavy Metals Ions. *J. Fiber Bioeng. Inf.* **2019**, *12*, 103−128.

(10) Liu, B.; Wang, D.; Yu, G.; Meng, X. Adsorption of Heavy Metal Ions, Dyes and Proteins by Chitosan Composites and Derivatives—A Review. *J. Ocean Univ. China* **2013**, *12*, 500−508.

(11) Menazea, A. A.; Ezzat, H. A.; Omara, W.; Basyouni, O. H.; Ibrahim, S. A.; Mohamed, A. A.; Tawfik, W.; Ibrahim, M. A. Chitosan/Graphene Oxide Composite as an Effective Removal of Ni, Cu, As, Cd and Pb from Wastewater. *Comput. Theor. Chem.* **2020**, *1189*, 112980.

(12) Abomosallam, M.; Elalfy, M.; Zheng, Z.; Nagata, K.; Suzuki, M. Adsorption Kinetics and Thermodynamics of Toxic Metal Ions onto Chitosan Nanoparticles Extracted from Shrimp Shells. *Nanotechnol. Environ. Eng.* **2022**, *7*, 35−47.

(13) Hoang, N. H.; Le Thanh, T.; Sangpueak, R.; Treekoon, J.; Saengchan, C.; Thepbandit, W.; Papathoti, N. K.; Kamkaew, A.; Buensanteai, N. Chitosan Nanoparticles-Based Ionic Gelation Method: A Promising Candidate for Plant Disease Management. *Polymers* **2022**, *14*, 662.

(14) Ma, Z.; Garrido-Maestu, A.; Jeong, K. C. Application, Mode of Action, and in Vivo Activity of Chitosan and Its Micro- and Nanoparticles as Antimicrobial Agents: A Review. *Carbohydr. Polym.* **2017**, *176*, 257−265.

(15) Mazancová, P.; Némethová, V.; Treľová, D.; Kleščíková, L.; Lacík, I.; Rázga, F. Dissociation of Chitosan/Tripolyphosphate Complexes into Separate Components upon PH Elevation. *Carbohydr. Polym.* **2018**, *192*, 104−110.

(16) de Carvalho, F. G.; Magalhães, T. C.; Teixeira, N. M.; Gondim, B. L. C.; Carlo, H. L.; dos Santos, R. L.; de Oliveira, A. R.; Denadai, Â. M. L. Synthesis and Characterization of TPP/Chitosan Nanoparticles: Colloidal Mechanism of Reaction and Antifungal Effect on C. Albicans Biofilm Formation. *Mater. Sci. Eng. C* **2019**, *104*, 109885.

(17) Al-Ahmed, Z. A.; Aljohani, M. M.; Sallam, S.; Alkhatib, F. M.; Alaysuy, O.; Alsharief, H. H.; Shah, R.; El-Metwaly, N. M. Synthesis of Magnetic Ruthenium Metal-Organic Frameworks for Efficient Removal of 2,4-Dichlorophenylacetic Pesticide from Aqueous Solutions: Batch Adsorption, Box-Behnken Design Optimization and Reusability. *J. Water Process Eng.* **2023**, *56*, 104444.

(18) Abumelha, H. M.; Alzahrani, S. O.; Alrefaee, S. H.; Al-bonayan, A. M.; Alkhatib, F.; Saad, F. A.; El-Metwaly, N. M. Evaluation of Tetracycline Removal by Magnetic Metal Organic Framework from Aqueous Solutions: Adsorption Isotherm, Kinetics, Thermodynamics, and Box-Behnken Design Optimization. *J. Saudi Chem. Soc.* **2023**, *27*, 101706.
(19) Alkhamis, K. M.; Aljohani, M. M.; Ibarhiam, S. F.; Hameed, Y. A. S.; Abumelha, H. M.; Habeebullah, T. M.; El-Metwaly, N. M. Application of Metal-Organic Frameworks for Efficient Removal of Doxorubicin Hydrochloride: Removal Process Optimization and Biological Activity. *ACS Omega* **2023**, *8*, 30374−30388.
(20) Sallam, S.; Aljohani, M.; Alatawi, N. M.; Alsharief, H.; Ibarhiam, S. F.; Almahri, A.; Alnoman, R. B.; El-Metwaly, N. M. Box-Behnken Design Optimization of Bimetallic-Organic Frameworks for Effective Removal of Tartrazine Food Dye from Aqueous Solutions. *J. Mol. Liq.* **2024**, *393*, 123667.
(21) Alzahrani, S. O.; Alsharief, H. H.; Alkhatib, F.; Alkhamis, K.; Sallam, S.; Abualnaja, M. M.; Saad, F. A.; El-Metwaly, N. M. Remarkable Remove of Sulfa Drugs from Water by One-Pot Synthesized Recyclable Composite Based on Wool and (Co & Ni)-BTC. *Inorg. Chem. Commun.* **2023**, *158*, 111695.
(22) Abualnaja, M. M.; Almotairy, A. R. Z.; Alorabi, A. Q.; Alaysuy, O.; Almahri, A.; Alkhamis, K.; Alrefaee, S. H.; El-Metwaly, N. M. Optimizing Cellulose Nanofiber Composite for Co2+ Ions Recovery from Lithium-Ion Battery Wastes and Removal from Wastewater: A Green Environmental Solution. *J. Water Process Eng.* **2024**, *57*, 104621.
(23) Promkatkaew, M.; Boonsri, P.; Hannongbua, S. Structural and Spectroscopic Properties of Metal Complexes with Ruhemann's Purple Compounds Calculated Using Density Functional Theory. *Key Eng. Mater.* **2019**, *824*, 204−211.
(24) Promkatkaew, M.; Kitjaruwankul, S.; Baiya, S.; Tongwanichniyom, S.; Boonsri, P.; Hannongbua, S. A DFT-Based Analysis of Metals Adsorption on Chitosan Monomer. *SWU. Sci. J.* **2022**, *38*, 37−47.
(25) Lee, S. X.; Tan, C. H.; Mah, W. L.; Wong, R. C. S.; Sim, K. S.; Cheow, Y. L.; Ng, C.-H.; Tan, K. W. Synthesis of Phenanthroline-Based Ligand and Its UV Activable Tetracarbonyl PhotoCORMs Based on Chromium, Molybdenum, and Tungsten as Cytotoxic and Antimicrobial Agents. *J. Organomet. Chem.* **2021**, *954*−*955*, 122103.
(26) Bencini, A.; Lippolis, V. 1,10-Phenanthroline: A Versatile Building Block for the Construction of Ligands for Various Purposes. *Coord. Chem. Rev.* **2010**, *254*, 2096−2180.
(27) Al-Omair, M. A. Biochemical Activities and Electronic Spectra of Different Cobalt Phenanthroline Complexes. *Arab. J. Chem.* **2019**, *12*, 1061−1069.
(28) Phillips, J. C.; Hardy, D. J.; Maia, J. D. C.; Stone, J. E.; Ribeiro, J. V.; Bernardi, R. C.; Buch, R.; Fiorin, G.; Hénin, J.; Jiang, W.; et al. Scalable Molecular Dynamics on CPU and GPU Architectures with NAMD. *J. Chem. Phys.* **2020**, *153*, 044130.
(29) Zoete, V.; Cuendet, M. A.; Grosdidier, A.; Michielin, O. SwissParam: A Fast Force Field Generation Tool for Small Organic Molecules. *J. Comput. Chem.* **2011**, *32*, 2359−2368.
(30) Humphrey, W.; Dalke, A.; Schulten, K. VMD: Visual Molecular Dynamics. *J. Mol. Graph.* **1996**, *14*, 33−38.
(31) Mark, P.; Nilsson, L. Structure and Dynamics of the TIP3P, SPC, and SPC/E Water Models at 298 K. *J. Phys. Chem. A* **2001**, *105*, 9954−9960.
(32) Darden, T.; York, D.; Pedersen, L. Particle Mesh Ewald: An $N \cdot \log(N)$ Method for Ewald Sums in Large Systems. *J. Chem. Phys.* **1993**, *98*, 10089−10092.
(33) Ryckaert, J.-P.; Ciccotti, G.; Berendsen, H. J. C. Numerical Integration of the Cartesian Equations of Motion of a System with Constraints: Molecular Dynamics of n-Alkanes. *J. Comput. Phys.* **1977**, *23*, 327−341.
(34) Hoover, W. G. Canonical Dynamics: Equilibrium Phase-Space Distributions. *Phys. Rev. A* **1985**, *31*, 1695−1697.
(35) Liu, H.; Hou, T. CaFE: A Tool for Binding Affinity Prediction Using End-Point Free Energy Methods. *Bioinformatics* **2016**, *32*, 2216−2218.
(36) Fatima, B. Quantitative Analysis by IR: Determination of Chitin/Chitosan DD. *Modern Spectroscopic Techniques and Applications*; IntechOpen, 2020.
(37) Leiva, W.; Toro, N.; Robles, P.; Gálvez, E.; Jeldres, R. I. Use of Multi-Anionic Sodium Tripolyphosphate to Enhance Dispersion of Concentrated Kaolin Slurries in Seawater. *Metals* **2021**, *11*, 1085.
(38) Abukhadra, M. R.; Refay, N. M.; El-Sherbeeny, A. M.; El-Meligy, M. A. Insight into the Loading and Release Properties of MCM-48/Biopolymer Composites as Carriers for 5-Fluorouracil: Equilibrium Modeling and Pharmacokinetic Studies. *ACS Omega* **2020**, *5*, 11745−11755.
(39) Ioelovich, M. Crystallinity and Hydrophility of Chitin and Chitosan. *Res. Rev.: J. Chem.* **2014**, *3*, 7−14.
(40) Kumar, S.; Koh, J. Physiochemical, Optical and Biological Activity of Chitosan-Chromone Derivative for Biomedical Applications. *Int. J. Mol. Sci.* **2012**, *13*, 6102−6116.
(41) Vimal, S.; Taju, G.; Nambi, K. S. N.; Abdul Majeed, S.; Sarath Babu, V.; Ravi, M.; Sahul Hameed, A. S. Synthesis and Characterization of CS/TPP Nanoparticles for Oral Delivery of Gene in Fish. *Aquaculture* **2012**, *358*−*359*, 14−22.
(42) Safdar, R.; Omar, A. A.; Arunagiri, A.; Thanabalan, M. Synthesis and Characterization of Imidazolium ILs Based Chitosan-Tripolyphosphate Microparticles. *IOP Conf. Ser.: Mater. Sci. Eng.* **2018**, *458*, 012080.
(43) Abdel-Raouf, M. E.-S.; Farag, R. K.; Farag, A. A.; Keshawy, M.; Abdel-Aziz, A.; Hasan, A. Chitosan-Based Architectures as an Effective Approach for the Removal of Some Toxic Species from Aqueous Media. *ACS Omega* **2023**, *8*, 10086−10099.
(44) O'Brien, J. T.; Williams, E. R. Coordination Numbers of Hydrated Divalent Transition Metal Ions Investigated with IRPD Spectroscopy. *J. Phys. Chem. A* **2011**, *115*, 14612−14619.
(45) Kollman, P. A.; Massova, I.; Reyes, C.; Kuhn, B.; Huo, S.; Chong, L.; Lee, M.; Lee, T.; Duan, Y.; Wang, W.; et al. Calculating Structures and Free Energies of Complex Molecules: Combining Molecular Mechanics and Continuum Models. *Acc. Chem. Res.* **2000**, *33*, 889−897.
(46) Holst, M.; Baker, N.; Wang, F. Adaptive Multilevel Finite Element Solution of the Poisson-Boltzmann Equation I. Algorithms and Examples. *J. Comput. Chem.* **2000**, *21*, 1319−1342.

https://doi.org/10.1021/acsomega.3c08835
ACS Omega 2024, 9, 4019−4026